


## ORIGINAL RESEARCH PAPER

# Co–Sn–Cu oxides/graphene nanocomposites as green catalysts for preparing 1,8-dioxo-octahydroxanthenes and apoptosis-inducing agents in MCF-7 human breast cancer cells

Kaveh Parvanak Boroujeni<sup>1</sup>  | Zeinab Tohidiyan<sup>2</sup> | Zahra Lorigooini<sup>3</sup> | Zahra Hamidifar<sup>1</sup> | Mohammad Mehdi Eskandari<sup>4</sup>

<sup>1</sup>Department of Chemistry, Shahrekord University, Shahrekord, Iran

<sup>2</sup>Department of Chemistry, Shahrekord Branch, Islamic Azad University, Shahrekord, Iran

<sup>3</sup>Medical Plants Research Center, Basic Health Sciences Institute, Shahrekord University of Medical Sciences, Shahrekord, Iran

<sup>4</sup>Nanotechnology Research Center, Research Institute of Petroleum Industry, Tehran, Iran

**Correspondence**

Kaveh Parvanak Boroujeni, Department of Chemistry, Shahrekord University, Shahrekord, Iran.  
Email: [parvanak-ka@sci.ac.ir](mailto:parvanak-ka@sci.ac.ir)

**Abstract**

In this work, Co–Sn–Cu oxides/graphene nanocomposite,  $30\text{--}40 \pm 0.5$  nm in size, was synthesized by solid-state microwave irradiation. This method presents several advantages such as operational simplicity, fast, low cost, safe and energy efficient, and suitability for production of high purity of nanoparticles. Other advantages of this method are there is no need for the use of solvent, fuel, and surfactant. Co–Sn–Cu oxides/graphene nanocomposites have been characterized by Fourier transform infrared spectroscopy, X-ray diffraction, field emission scanning electron microscopy, transmission electron microscopy, vibrating sample magnetometer, energy-dispersive X-ray spectroscopy, and UV–Vis spectroscopy. The synthesized nanocomposites were used as novel highly efficient catalysts for the synthesis of 1,8-dioxo-octahydroxanthenes at room temperature. The catalysts are recoverable and can be reused for six runs without loss of their activity. Also, the obtained nanocomposites exhibited significant anticancer activity against breast cancer cells and they could induce apoptosis in cancer cells.

## 1 | INTRODUCTION

Graphene and graphene oxide (GO) have been widely used to fabricate various kinds of composite materials and also for catalysis synthesis due to their high surface area, high chemical stability, strong conductivity for electron transfer, and low cost [1, 2]. Among these, graphene supported metal nanocomposites has received more attention [3]. For example, bimetallic Sn–W oxides/graphene and tin–zirconia/graphene nanocomposites have been reported as heterogeneous catalysts for selective oxidation of alcohols [4] and synthesis of dimethyl carbonate [5], respectively. However, despite many examples of immobilized metal nanocomposites, little is established on their usage as a catalyst in organic transformations.

Natural products with a xanthene moiety have revealed biological activities such as anti-inflammatory [6], anti-bacterial [7], and anti-cancer activities [8] (Scheme 1). 1,8-Dioxo-octahydroxanthenes are one of the most important derivatives of xanthenes which were usually synthesized via one-pot Knoevenagel condensation, Michael addition, and

cyclodehydration of 5,5-dimethyl-1,3-cyclohexanedione (dime-tinqh\_9;done) with various aldehydes. Numerous Lewis and Brönsted acid catalysts have been used to promote this reaction [9–20]. Although these catalysts are suitable for certain synthetic conditions, their main disadvantages are long reaction times, tedious work-up, the formation of uncyclized adduct 2,2'-aryl-methylene bis(3-hydroxy-2-cyclohexene-1-one), and the use of unrecyclable, hazardous, or difficult to handle catalysts. The need to high temperatures [9–16] or an additional energy (ultrasound or microwave) [17, 18] is another drawback of many of these methods. These reactions are rarely carried out at low temperature [19, 20]. Hence, the development of new catalysts with more efficiency is still in demand.

Transition metals have been received much attention from the biological point of view because they are the key linkers of complex proteins or enzymes [21, 22]. The mechanism of action of the bivalent cationic metalloestrogens in breast cancer has been reviewed recently [23]. Metal-based compounds including copper and tin have been surveyed with promising chemotherapeutic potential for the treatment of a range of

This is an open access article under the terms of the Creative Commons Attribution License, which permits use, distribution and reproduction in any medium, provided the original work is properly cited.

© 2021 The Authors. *IET Nanobiotechnology* published by John Wiley & Sons Ltd on behalf of The Institution of Engineering and Technology.

cancers [24–27]. Because of the great potential of copper and tin complexes as anticancer agents, complexes made up of both metals have attracted much attention due to a plausible dual mode of action at the molecular level [28]. For instance, the chiral L-tryptophan-derived [bis(1,2-diaminobenzene) copper (II)] chloride complex,  $\text{CuSn}_2(\text{Trp})$ , showed antitumor activity [29] as well as induced cytotoxicity in PA-1, PC-3, HeLa, U2OS, HepG2, and MCF-7 cancer cell lines [30]. In addition, cobalt-based ligand complexes have a wide spectrum of biological activities as antibacterial and antiviral properties [31]. Cobalt-doped magnetite, iron–cobalt/ferrite core–shell structures, and cubic iron–cobalt nanoparticles have been used for hyperthermia application in cancer therapy [32–34]. Also, the efficiency of graphitic carbon–cobalt nanoparticles as localized radio frequency absorbers for cancer treatment has been investigated [35].

Breast cancer is one of the main health concerns facing our society and is the second leading cause of morbidity and mortality among women worldwide [36]. For clinical treatment of breast cancer, in many occasions chemotherapy is one important option. Nanotechnology is on the route to providing novel developments in medicine science, such as designing biocompatible inorganic nanomaterials with applications of determination of drug [37] and anti-oxidant [38], anti-bacterial [39], and anti-biofilm properties [40]. In addition, nanotechnology has attracted attention in tumor imaging and cancer therapy and in this regard nanoparticles with many unique properties, such as a high surface area-to-volume ratio and magnetic and optical properties, play important roles [41]. In this regard, the graphene-based nanomaterials have attracted considerable interest in upcoming nanotechnology-based medicine applications [42]. For instance, GO as a carrier for adriamycin in cancer drug resistance [43] and the effect of curcumin-reduced GO on breast cancer cells [44] have been investigated. GO–silver nanocomposite [45] and gallic acid/CdS on the GO nanosheets [46] were used for targeted therapy of human ovarian cancer stem cells and treatment of kidney tumor cells, respectively. Tamoxifen citrate on reduced GO nanosheets was used for breast cancer therapy [47]. Also, Zhou et al. applied platinumated GO nanostructure for efficient gene-chemo combination cancer therapy [48]. The hydrophilic graphene-based yolk-shell magnetic nanoparticles functionalized with copolymer pluronic F-127 (GYSMNP@PF127) has been reported as an efficient multifunctional biomedical system for mild hyperthermia and stimuli–responsive drug delivery [49].

Various synthetic techniques have been reported for preparing metal nanocomposites, including sonochemical [50], thermal decomposition [51], hydrothermal [52], and sol-gel methods [53]. In this regard, the important issue for choosing synthetic method is reducing the cost of physical and chemical synthesis route; meanwhile, it can produce nanocomposites with high purity in short time. Solid-state microwave-assisted method with controlling time and reaction temperature quite provides these main purposes and is able to generate nanocomposites in narrow particle size distribution [54]. Along this line and in the continuation of our recent works on synthesis of NiO nanoparticles using solid-state microwave-assisted

method [55] and investigation of biological activity [39, 56, 57] and drug determination [37] of the synthetic compounds, the synthesis of Co–Sn–Cu oxides/graphene nanocomposites by solid-state microwave irradiation and their use as novel catalysts for preparing 1,8-dioxo-octahydrozantenes are reported. Also, the anti-proliferative activity and apoptosis induction of nanocomposites on a breast cancer cell line is investigated.

## 2 | EXPERIMENTAL SECTION

### 2.1 | Materials and methods

All chemicals were either prepared in our laboratory or were purchased from Merck and Fluka. Reaction monitoring and purity determination of the products were accomplished by gas liquid chromatography or thin-layer chromatography (TLC) on silica-gel polygram SILG/UV254 plates. Gas chromatography was carried out on Shimadzu GC 14–A.  $^1\text{H}$  NMR spectra were recorded on 400 MHz spectrometer in  $\text{CDCl}_3$ . Melting points were determined on a Fisher–Jones melting-point apparatus. To determine the crystalline phase, powder X-ray diffraction (XRD) analysis was carried on an X-ray diffractometer with Ni-filtered  $\text{Cu K}\alpha$  irradiation ( $\lambda = 1.54 \text{ \AA}$ ), for an angle range of  $2\theta = 10\text{--}80^\circ$ . Infrared spectrum was carried on a Fourier transform infrared (FT–IR) 160 spectrophotometer (Shimadzu system) by KBr tablets. UV–Vis spectroscopy measurement at room temperature (298 K) was obtained by a double-beam Shimadzu 1650 PC. The powder samples for UV–Vis analysis were dispersed in EtOH for 25 min to make a homogeneous suspension. Field emission scanning electron microscopic (FESEM) images were taken on a Hitachi s4160/Japan equipped with a link energy dispersive X-ray (EDX) analyzer with gold coating. Transmission electron microscopy (TEM, Philips CM10) was applied at accelerating voltage of 300 kV. The sample was sonicated in EtOH, and a drop of the suspension was dried on a carbon-coated microgrid for the TEM analysis. The magnetic property of the sample was measured at room temperature (298 K) using a vibrating sample magnetometer (VSM, MDKFD, Meghnatis Kavir Kashan Co.). Ultrasonic generator was carried out on ultrasonic probe (Top-Sonics UPH-400, ultrasonic technology development Co.). A microwave oven (LG, 2.45 GHz, 900 W) was used for the microwave irradiation. For anticancer study, data were analyzed by SPSS using the Kruskal–Wallis test and are presented as the means  $\pm$  standard deviation from at least three independent experiments. The apoptosis was examined by flow cytometry (Partec System, Germany). IC50 value was calculated using probit analysis.

### 2.2 | Synthesis of Schiff base ligand (H2L)

4,4'-Dibromo-2,2'-[cyclohexane-1,2-diylbis(nitrilomethanylylidene)]diphenol (H2L) was synthesized according to our previous study [56]. 1,2-Diaminocyclohexane (0.1 g, 1 mmol) was added to 5-bromosalicylaldehyde (0.4 g, 2 mmol) in 20 mL MeOH. The mixture was refluxed for 1 h. The yellow powder

was filtered off, washed with cold methanol, and dried under vacuum over anhydrous  $\text{CaCl}_2$ .

### 2.3 | Synthesis of precursor powders

Three solutions of H2L ligand (0.3 mmol, 0.15 g) in methanol (10 mL) were exposed to ultrasonic irradiation, and 10 mL of a methanolic solution of  $\text{Cu}(\text{CH}_3\text{COO})_2 \cdot 2\text{H}_2\text{O}$  (0.14 g, 0.3 mmol) was added to each solution in a dropwise manner [57]. Then, 0.1 mmol of  $\text{Co}(\text{NO}_3)_2 \cdot 5\text{H}_2\text{O}$  with different amounts of  $\text{SnCl}_2 \cdot 2\text{H}_2\text{O}$  (0.005, 0.01, or 0.02 mmol) dissolved into 20 mL of methanol was added to each above mixture under ultrasonic irradiation (300 W) for 20 min at room temperature to form a homogeneous light brown solution. When the pH of each mixture was adjusted to 11 by NaOH aqueous solution (1 M), a precipitate was formed which was then filtered off, washed with cold methanol, and dried under vacuum over anhydrous  $\text{CaCl}_2$ . Three obtained powders were used as precursors for the preparation of corresponding Co–Sn–Cu oxides/graphene nanocomposites.

### 2.4 | Synthesis of Co–Sn–Cu oxides nanocomposites

To prepare Co–Sn–Cu oxides/graphene nanocomposites, in separate tests, 2 g of the above precursor samples was added to a porcelain crucible and each one was placed in another bigger porcelain crucible that is filled with CuO powder (microwave absorber). The assembly was placed in a microwave oven and exposed to microwave irradiation at 900 W (100%) in air. Along irradiation, temperature of CuO powder increased from room temperature to 450°C. The temperature was determined by a chromel–alumel thermocouple in the mixture vessel. The generated heat was transferred to precursor sample and it was decomposed. After 10 min, decomposition of each powder was completed. The obtained products were cooled to room temperature, washed with ethanol, and dried under vacuum over anhydrous  $\text{CaCl}_2$  to produce three Co–Sn–Cu oxide nanocomposites.

### 2.5 | Synthesis of GO

A double-jacket reactor was charged with 85% phosphoric acid (10 mL), and the circulator temperature was adjusted at 5°C. Then, concentrated sulfuric acid (90 mL) was added to the mixture and stirred. A well-ground mixture of graphite (1 g, particle size <50  $\mu\text{m}$ ) and potassium permanganate (5 g) was gradually added into the above solution over a period of 2 h, and the mixture was stirred at 5°C for 3 h. Afterwards, the mixture was stirred with stepwise temperature rise to 25°C for 3 h and then to 55°C in 2 h. After that, the mixture was stirred at 55°C for 12 h, cooled to 5°C, and finally poured into crushed ice and stirred. To the resulting mixture, hydrogen peroxide (30%) was added slowly until an ochre color was

achieved. The precipitate formed was collected by filtration, washed twice with 50 mL of deionized water and then with concentrated hydrochloric acid ( $2 \times 10$  mL). The washing was repeated with deionized water until sulfate and manganese ions were no longer present in the eluate (checked by barium and sodium bismuthate tests). Finally, the GO product was washed with ethanol and acetone and dried under vacuum at 70°C overnight [58].

### 2.6 | Synthesis of reduced GO from GO

Reduced graphene oxide (rGO) was synthesized through the previously reported method [59]. To a suspension of GO (500 mg) in water (20 mL) was added 50 mL of hydrazine monohydrate. The mixture was refluxed for 24 h at 100°C. The obtained powder was washed with water and ethanol and dried under vacuum over anhydrous  $\text{CaCl}_2$ .

### 2.7 | Synthesis of Co–Sn–Cu oxides/graphene nanocomposites (1, 2, and 3)

In separated tests, to 20 mL of ethanolic suspension of the three above prepared Co–Sn–Cu oxides nanocomposites (0.1 g), 10 mL of ethanolic solution of rGO (0.1 mg) was added dropwise and stirred at 90°C for 30 min and it was exposed to ultrasonic irradiation (250 W) for 10 min. The formed powders were separated by centrifugation and dried at 120°C for 12 h. The obtained products were named nanocomposites 1–3 based on tin concentration of 0.005, 0.01, and 0.02 mmol, respectively.

### 2.8 | Typical procedure for preparing 1,8-dioxo-octahydroxanthenes

A mixture of 3-nitrobenzaldehyde (1 mmol), dimedone (2 mmol), nanocomposite 3 (0.01 g), and ethanol/water (3 mL, 1:1) was prepared and stirred at room temperature. After completion of the reaction (monitored by TLC), the catalyst was removed by an external magnet and washed with 5 mL of ethanol and the filtrate was concentrated on a rotary evaporator under reduced pressure to yield the corresponding product. Whenever required, the products were purified by recrystallization from ethanol.

### 2.9 | Cell culture and treatment

Normal and human breast cancer cells (MCF-7) were obtained from National Cell Bank of Iran (NCBI), Pasteur Institute of Iran (Tehran, Iran). The MCF-7 cells were cultured in standard condition (95% humidity, 5%  $\text{CO}_2$ , 37°C) in RPMI 1640 supplemented with 10% heat-inactivated fetal bovine serum. A 200 mM solution of each nanocomposite (1–3) in 100% dimethyl sulfoxide (DMSO) and different concentrations was

prepared with the RPMI 1640; the final concentration of DMSO was less than 0.02% in both control and treated cells.

## 2.10 | Cell viability assay

MCF-7 were seeded in a concentration of  $8 \times 10^3$  cells per well in 96-well plates for 24 h before treatment and exposed to different concentrations of nanocomposites (0–500  $\mu\text{g}/\text{mL}$ ) for 24 and 48 h. Cell viability was then examined by the colorimetric assay using the 3-(4,5-dimethylthiazol-2-yl)-2,5-diphenyltetrazolium bromide (MTT) assay, according to the manufacturer's instruction (Sigma Aldrich, USA). Briefly, after different incubation times, cells were washed twice with phosphate-buffered saline (PBS) and MTT solution prepared in PBS (5 mg/mL) was added to each well to the final concentration of 0.5 mg/mL in no-phenol red RPMI and was incubated for 3 h in a dark place. After washing with PBS, 100  $\mu\text{L}$  of DMSO was added to each well, and absorbance was measured at 570 nm by an Elisa reader (stat fax-2100 awareness). Viability of each group was measured according to the absorbance compared with control.

## 2.11 | Apoptosis assay

MCF-7 cells were seeded in 6-well plates at a density of  $1 \times 10^6$  cells per well, grown for 24 h before treatment with nanocomposites at IC50 value for 48 h. The apoptosis was examined by flow cytometry using the Annexin V-FITC/propidium iodide (PI) apoptosis kit (BD Biosciences), according to the manufacturer's instruction. Briefly, MCF-7 cells were washed with cold PBS and were then resuspended in 1 mL of 1x binding buffer (provided with kit) at density of  $10 \times 10^6$  cells/mL. 100  $\mu\text{L}$  of cell suspension was incubated with 5  $\mu\text{L}$  of Annexin V-FITC and PI for 20 min in the dark at room temperature, and then examined by flow cytometry. The percentage of cells in different stages (apoptosis and necrosis) was examined by FlowJo 7.6 software. At least 12,000 events were recorded and represented as dot plots.

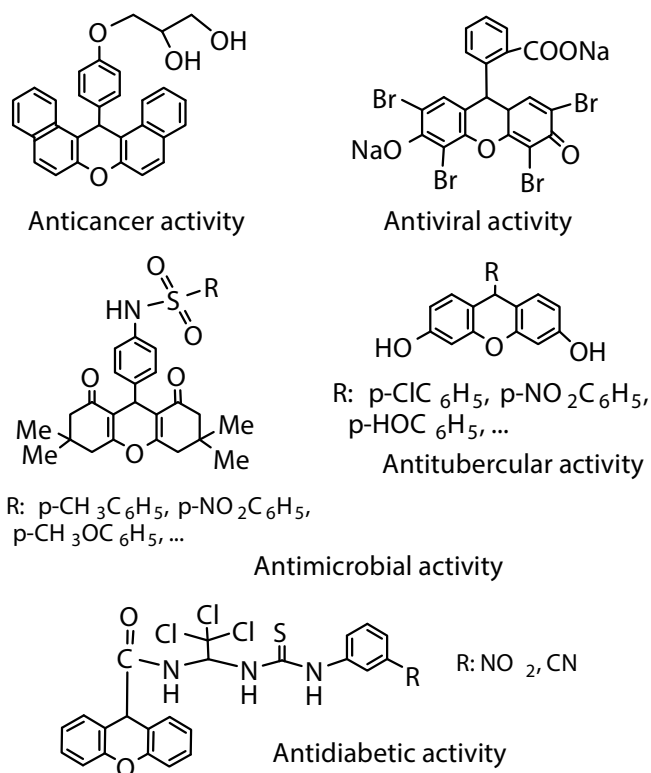
## 3 | RESULTS AND DISCUSSION

### 3.1 | Synthesis and structural characterization of nanocomposites

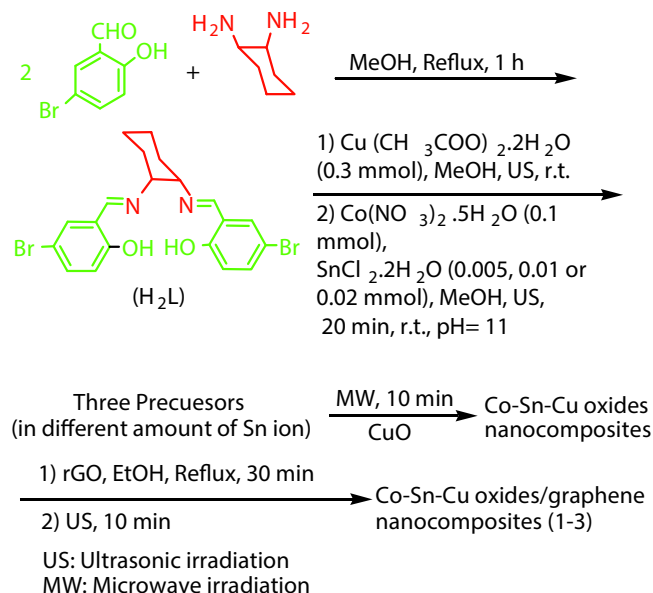
By solid-state microwave irradiation, three nanocomposites (1, 2, and 3) were prepared in a short time (Scheme 2). For this purpose, first a Schiff base ligand ( $\text{H}_2\text{L}$ ) was prepared using 1,2-diaminocyclohexane and 5-bromosalicylaldehyde which was then reacted with  $\text{Cu}(\text{CH}_3\text{COO})_2 \cdot 2\text{H}_2\text{O}$ ,  $\text{Co}(\text{NO}_3)_2 \cdot 5\text{H}_2\text{O}$ , and  $\text{SnCl}_2 \cdot 2\text{H}_2\text{O}$  at different concentrations to produce three precursors. Afterwards, each precursor was exposed to microwave irradiation to yield their corresponding nanocomposites. However, we observed that the precursors remained unchanged for 30 min, indicating that

they do not absorb microwaves energy. Therefore, reaction requires a secondary irradiation absorber. For this purpose, CuO powder was used. Then, each precursor was completely decomposed through the absorption of heat from the hot CuO and the corresponding nanosized Co–Sn–Cu oxides/graphene nanocomposites were formed. Decomposition of each precursor was accompanied by the release of different gases such as  $\text{N}_2$ ,  $\text{NO}$ ,  $\text{N}_2\text{O}$ , and  $\text{H}_2\text{O}$  vapors. After the synthesis of nanocomposites, the Co–Sn–Cu oxides/graphene nanocomposite 3 (with 0.02 mmol of Sn ion, abbreviated hereinafter to nanocomposite 3) was considered as representative sample for characterization by different analyses.

Figure 1(a) shows XRD pattern of the corresponding precursor for nanocomposite 3. This pattern manifested that the particles were in nanometer scale. The main diffraction peaks were observed at  $2\theta = 27.1705^\circ$  and  $45.0807^\circ$ . The average particle size was calculated to be about 42.72 nm, by applying a full width at half maximum and the value of  $2\theta$  of the characteristic peak of the XRD pattern using the Debye–Scherrer equation [60]. Figure 1(b) displays the XRD pattern of nanocomposite 3 at the power level of 900 W for 10 min in a microwave cavity. All the diffraction peaks of the XRD pattern could be indexed to the monoclinic CuO phase (space group:  $\text{C}2/c$ ; No. 15, JCPDS Card No. 80-1268) at  $2\theta = 35.5806^\circ$ ,  $38.7820^\circ$ , and  $48.8044^\circ$ , which can be perfectly related to  $(-1\ 1\ 1)$ ,  $(1\ 1\ 1)$ , and  $(-2\ 0\ 2)$  crystal planes, respectively. Lattice constants of the CuO phase were calculated to be  $a = 4.68$ ,  $b = 3.42$ , and  $c = 5.12$  nm. Also,



**SCHEME 1** Biological applications of a series of xanthene derivatives



**SCHEME 2** The synthetic routes for Co–Sn–Cu oxides/graphene nanocomposites

diffraction peaks of Co<sub>3</sub>O<sub>4</sub> (JCPDS Card No. 74-2120) and SnO<sub>2</sub> phases (JCPDS Card No. 88-0287) were observed in this pattern. As shown in Figure 1(b), no amorphous phase, composed of rGO, was detected [61]. No characteristic XRD peaks arising from precursor were observed, indicating the formation of pure nanocomposite 3. The average particle size of the synthesized nanocomposite 3 was determined using the Debye–Scherrer formula to be 33.92 nm.

The FT–IR spectra of nanocomposite 3 and its corresponding precursor are shown in Figure 2. In IR spectrum of the precursor (Figure 2(a)), the band at 1607.72 cm<sup>-1</sup> is related to the azomethine group (C=N) which has shifted to a lower frequency compared to the copper (II) complex of Schiff base ligand (H<sub>2</sub>L) (1630 cm<sup>-1</sup>) [57] due to the presence of cobalt and tin in the compound. In the IR spectrum of nanocomposite 3 (Figure 2(b)), a strong band was observed at around 571 cm<sup>-1</sup> which can be assigned to the M–O bond (M = Cu, Co, and Sn) [57, 62]. The C–H and C–O stretching vibrations due to graphene sheets appeared at 2925 and 1383 cm<sup>-1</sup>, respectively [63]. Also, the appearance of bands at 3432 and 1631 cm<sup>-1</sup> was assigned to the stretching and bending vibrations of the water molecules absorbed by the sample or KBr [57]. The disappearances all characteristic bands of the precursor in the IR spectrum of nanocomposite 3 demonstrated complete decomposition of the precursor into nanocomposite 3 by the solid-state microwave-assisted method.

The morphology of nanocomposites and their corresponding precursors were surveyed by the FESEM analysis (Figure 3). The FESEM images of the precursor of nanocomposite 3 show nanorods which were loosely aggregated

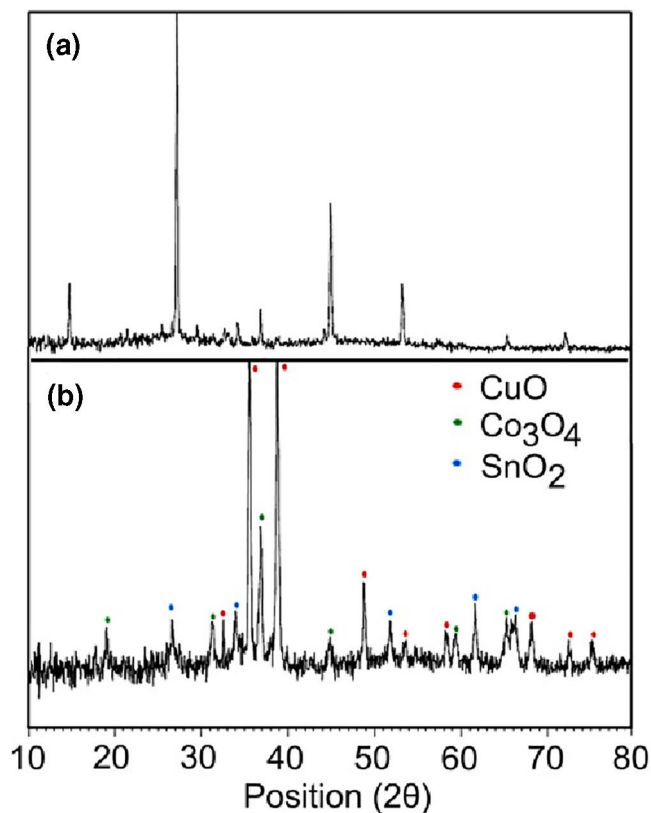


**FIGURE 1** XRD pattern of nanocomposite 3 (b) and its corresponding precursor (a)

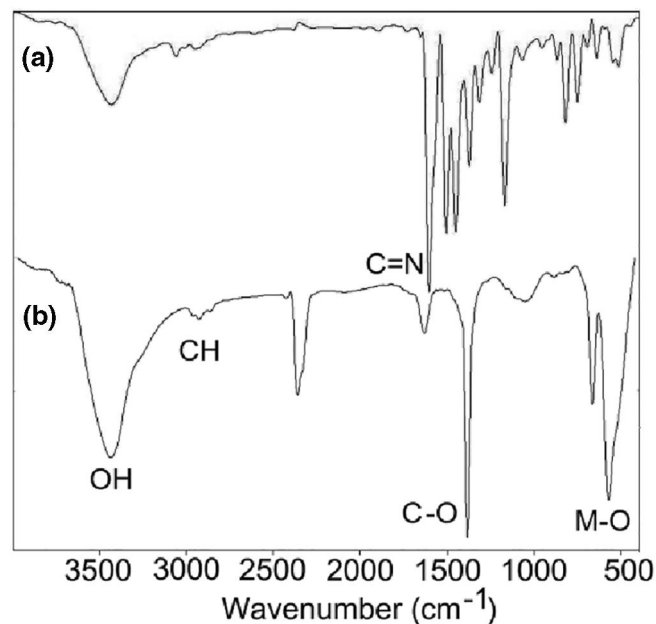


**FIGURE 2** FT–IR spectra of nanocomposite 3 (b) and its corresponding precursor (a)

(Figure 3(a) and (b)). As shown in Figure 3(c) and (d), the morphology of nanocomposite 3 is semispherical shape. The particle size distribution of the precursor and nanocomposite 3

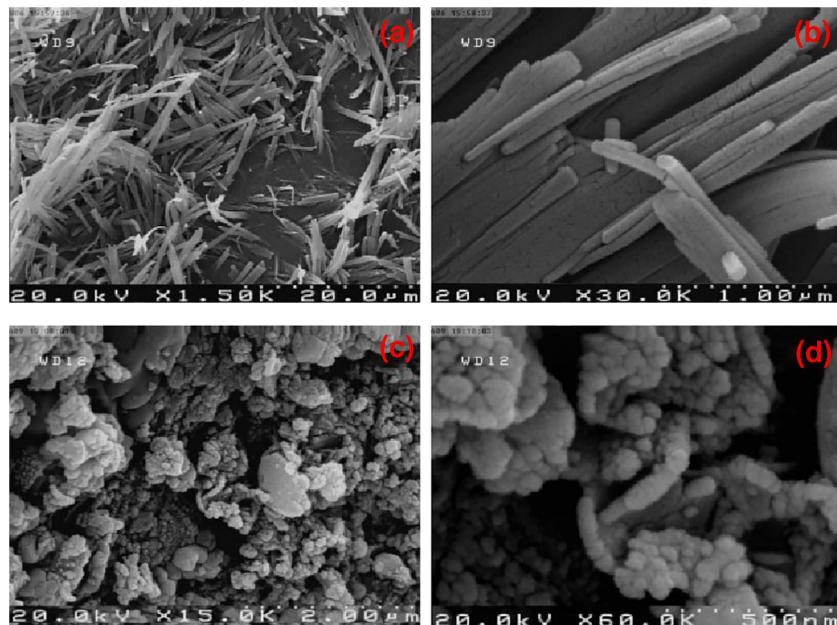


**FIGURE 3** FESEM images of the corresponding precursor for nanocomposite 3 (a, b) and nanocomposite 3 (c, d) at different magnifications

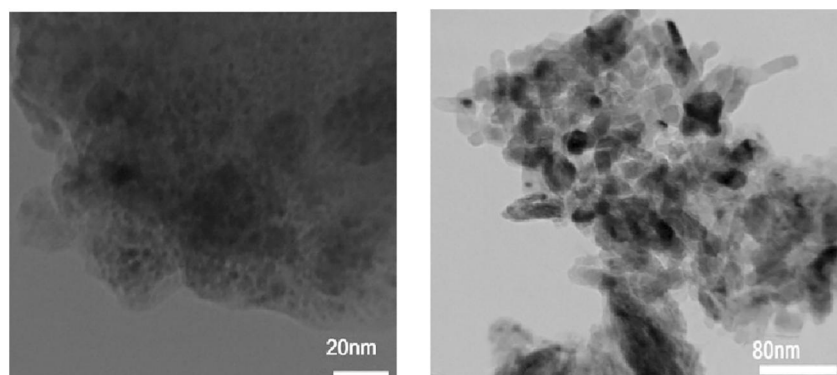


**FIGURE 4** TEM images of nanocomposite 3 at different magnifications

was found to be  $50\text{--}60 \pm 0.8$  and  $30\text{--}40 \pm 0.5$  nm, respectively. These results are in good agreement with the XRD analysis. The striking difference between the size and shape of nanocomposite 3 with its corresponding precursor showed that their structures are quite different and confirmed that decomposition of precursor into the product particles is complete. Therefore, solid-state microwave irradiation is a beneficial method for the synthesis of varied nano-sized compounds in high purity. The difference between this method and the conventional heating methods results from the difference in the mechanism of the reactions. The solid-state microwave irradiation involves converting electromagnetic energy into heat by fast kinetics of the molecules. The electromagnetic energy arises from interaction of microwave wavelengths with the reactants at the molecular level [64]. These extreme conditions lead to solid-state decomposition reactions and the formation of nano-sized particles in different morphologies.

The morphology and particle size of the synthesized nanocomposites were further investigated by TEM analysis.

TEM images of nanocomposite 3 are given in Figure 4 at different magnifications. The images showed the spherical shape of particles with the particle size distribution of  $30\text{--}40 \pm 0.5$  nm, similar to that obtained using the XRD and FESEM analysis.

Figure 5 shows the EDX analysis of nanocomposite 3 that confirms the presence of Co, Cu, Sn, C, and O elements in this nanocomposite. The Si and Au signals were observed due to the coating material of the instrument. Pleasingly, EDX results (inset in Figure 5) are in close agreement with the ratios used in the synthetic processes. Hence, these results show that nanocomposite 3 was prepared in high purity by the presented solid-state microwave method.

It is believed that the magnetic property of nanomaterials is highly dependent on the type of sample shape, size of particles, magnetization direction, and synthetic method. The variation in magnetization ( $M$ ) as a function of applied field ( $H$ ) at room temperature for nanocomposite 3 is depicted in Figure 6 and shows a superparamagnetic behavior of the nanocomposite ( $M_r = 0.24$  emu/g).

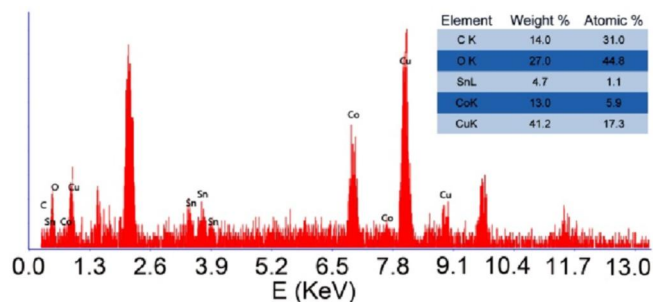


FIGURE 5 EDX spectrum of nanocomposite 3

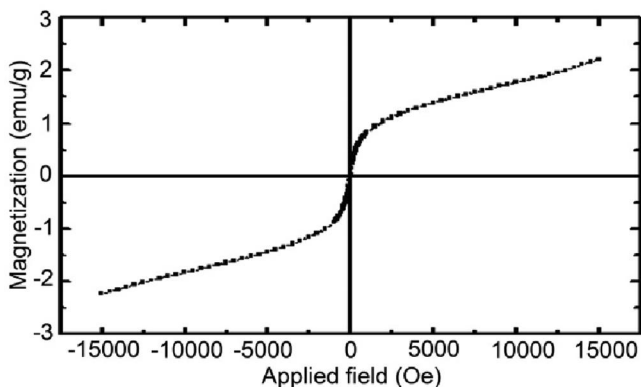


FIGURE 6 Magnetization versus applied magnetic field at room temperature for nanocomposite 3

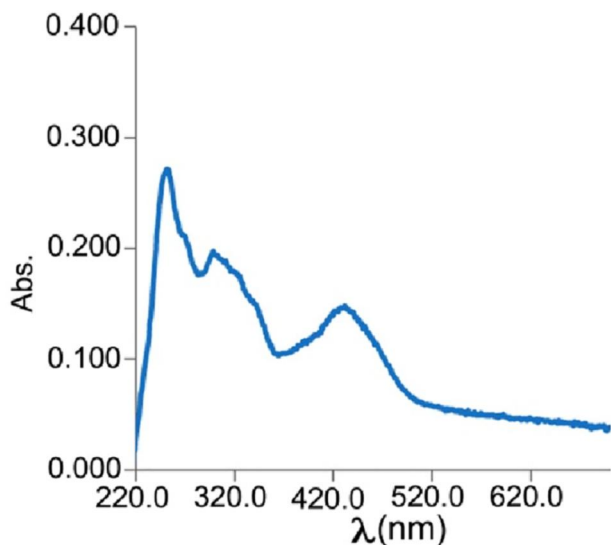


FIGURE 7 Electronic spectrum of the corresponding precursor of nanocomposite 3

The electronic property of the synthesized nanocomposites was surveyed by UV-Vis analysis. Figure 7 shows the electronic spectrum of the corresponding precursor for nanocomposite 3. The band at 247 nm was related to the  $\pi-\pi^*$

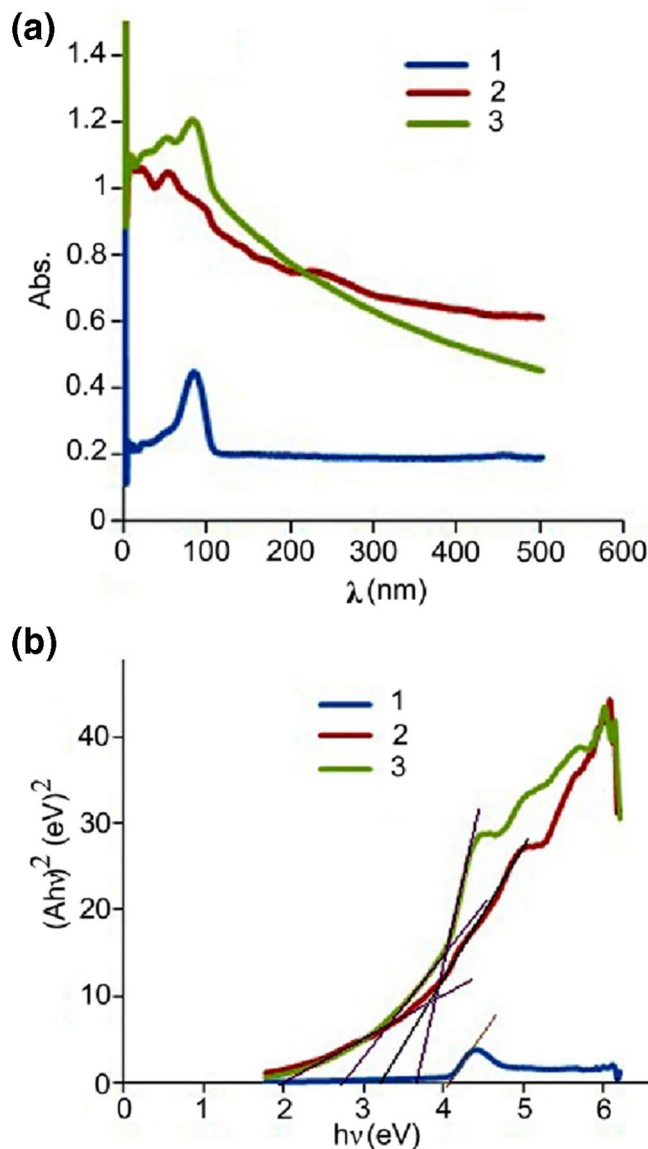
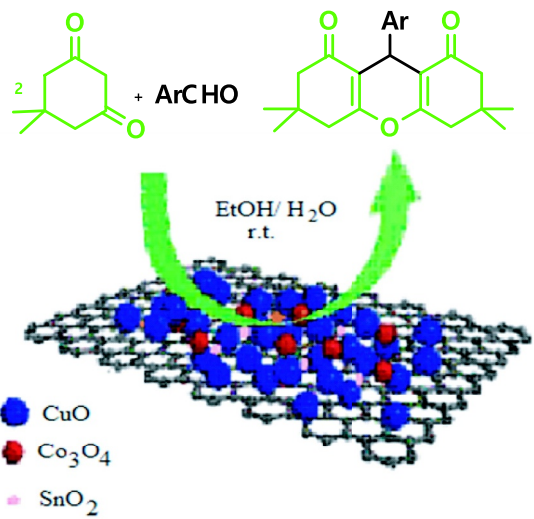


FIGURE 8 Electronic spectra of the nanocomposites 1–3 (assigned 1 (blue line), 2 (red line), and 3 (green line)) (a) and their corresponding  $(A\hbar\nu)^2 - \hbar\nu$  curves (b)

transition of the aromatic rings contained in ligand structure. The bands at 393–422 nm were attributed to the MLCT (metal ligand charge transfer) and LMCT (ligand metal charge transfer) transitions [65, 66]. These bands showed a shift toward the copper (II) complex of Schiff base ligand ( $H_2L$ ) [57] due to the presence of tin and cobalt ions.

Figure 8 shows electronic spectra and the  $(A\hbar\nu)^2 - \hbar\nu$  curves of the nanocomposites 1–3. In Figure 8(a), the observed bands ( $<200$  nm) of the nanocomposites are due to the electron transitions from Cu (3d) and O (2p) orbitals [67] and have highest intensity for nanocomposite 3. These bands showed a blue shift compared with pure CuO nanoparticles [68, 69], due to the presence of Co and Sn ions. The band gap ( $E_g$ ) of the synthesized nanocomposites can be obtained by the equation:  $(A\hbar\nu)^2 = B (\hbar\nu - E_g)$ , where A,  $\hbar\nu$ , and B represent the



**SCHEME 3** The catalytic performance of Co–Sn–Cu oxides/graphene nanocomposites in the green synthesis of 1,8-dioxo-octahydroxanthenes

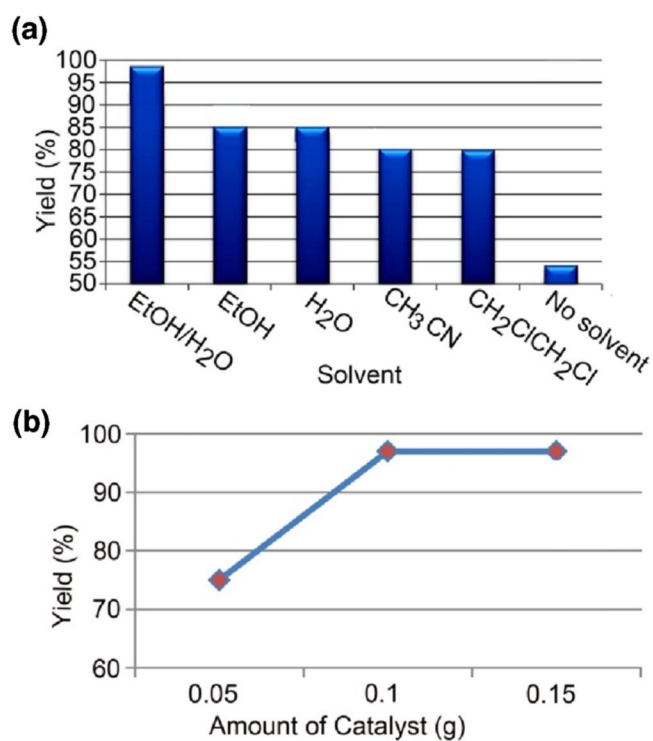


**FIGURE 9** The screening of the solvent nature (a) and catalyst amount (b) on the reaction of 4-bromobenzaldehyde (1 equivalent) with dimedone (2 equivalents) after 20 min at room temperature catalyzed by nanocomposite 3

absorption coefficient, the energy of photon, and a constant depending on the type of materials, respectively. Figure 8(b) shows the  $(A\text{h}\nu)^2 - h\nu$  curves for the nanocomposites 1–3. The band gaps of the nanocomposites 1–3 were estimated as 4.1, 3.7, and 3.8 eV, respectively, by extrapolation of the

**TABLE 1** Preparation of 1,8-dioxo-octahydroxanthenes from the reaction aldehydes with dimedone using nanocomposite 3<sup>a</sup>

No.	Ar	Time (min)	Yield (%) <sup>b</sup>	mp (°C) (lit.) [Ref.]
1	4-NO <sub>2</sub> C <sub>6</sub> H <sub>5</sub>	14	97	224–227 (226–228) [12]
2	3-NO <sub>2</sub> C <sub>6</sub> H <sub>5</sub>	15	97	167–170 (170–171) [11]
3	2,4-Cl <sub>2</sub> C <sub>6</sub> H <sub>4</sub>	18	96	250–253 (247–248) [11]
4	4-CNC <sub>6</sub> H <sub>5</sub>	16	96	213–217 (217–221) [19]
5	4-ClC <sub>6</sub> H <sub>5</sub>	19	95	225–229 (237–238) [11]
6	4-BrC <sub>6</sub> H <sub>5</sub>	20	97	235–237 (240–241) [11]
7	C <sub>6</sub> H <sub>5</sub>	20	96	199–203 (205–206) [11]
8		20	94	60–63 (62–63) [13]
9		20	94	160–163 (160–165) [19]
10	4-MeC <sub>6</sub> H <sub>5</sub>	22	93	210–213 (212–214) [10]
11	4-HOC <sub>6</sub> H <sub>5</sub>	22	93	238–241 (244–246) [10]
12	4-MeOC <sub>6</sub> H <sub>5</sub>	24	93	239–243 (242–245) [10]

<sup>a</sup>All reactions were carried out in EtOH/H<sub>2</sub>O (1:1) at room temperature in the presence of nanocomposite 3 (0.1 g).

<sup>b</sup>Isolated yield. All products are known compounds and were identified by comparison of their physical and spectral data with those of the authentic samples.

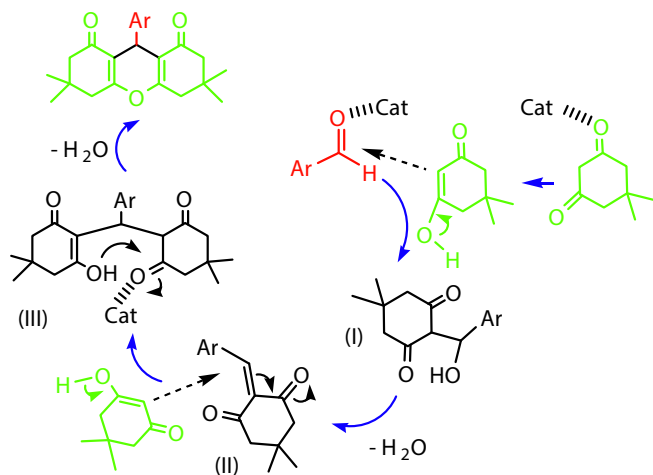
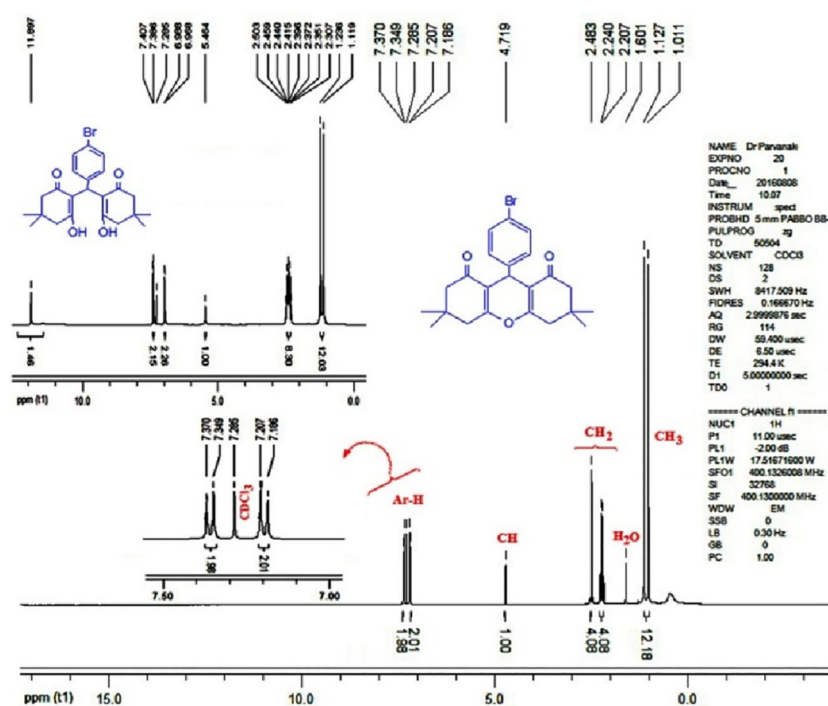
corresponding curves. The value of band gaps for three nanocomposites has a slight shift relative to each other, most probably due to their difference in particle size and the tin content. Based on these results, it can be predicted that the synthesized nanocomposites can be used as semiconductors.

### 3.2 | Catalytic application of the nanocomposites

After synthesis and characterization of the nanocomposites, their catalytic activity for preparing 1,8-dioxo-octahydroxanthenes was examined (Scheme 3). For this purpose, the condensation reaction of 4-bromobenzaldehyde with dimedone was chosen as a model reaction for the optimization of the reaction conditions. As it can be seen from Figure 9a,b, 3,4,6,7-tetrahydro-3,3,6,6-tetramethyl-9-(4-bromophenyl)-2H-xanthene-1,8(5H,9H)-dione product was obtained in 97% yield in EtOH/H<sub>2</sub>O (1:1) as green solvents after 20 min at room temperature in the presence of 0.1 g of nanocomposite 3. No significant difference was found between catalytic activities of nanocomposites 1–3. Thus, we typically applied this optimized condition for the reaction of a variety of aromatic aldehydes with dimedone in the presence of nanocomposite 3. The results showed that both aldehydes bearing electron-donating, electron-withdrawing, and halogen substituents gave the desired 1,8-dioxo-octahydroxanthenes in high-to-excellent yields (Table 1, entries 1–7, 10–12). Acid-sensitive aldehydes such as furan-2-carboxaldehyde and thiophene-2-carboxaldehyde (entries 8, 9) reacted well and gave the corresponding



**FIGURE 10**  $^1\text{H}$  NMR spectrum of 3,4,6,7-tetrahydro-3,3,6,6-tetramethyl-9-(4-bromophenyl)-2H-xanthen-1,8(5H,9H)-dione



**SCHEME 4** The proposed mechanism for the synthesis of 1,8-dioxo-octahydroxanthenes catalyzed by nanocomposite 3

products in high yields. In the absence of the catalyst, no products were formed. All the reactions were clean as indicated by TLC and the only work-up being the easy removal of the catalyst using an external magnet and then evaporation of reaction solvent. Figure 10 shows  $^1\text{H}$ -NMR spectrum of 3,4,6,7-tetrahydro-3,3,6,6-tetramethyl-9-(4-bromophenyl)-2H-xanthen-1,8(5H,9H)-dione.

A plausible mechanism for the condensation reaction of aromatic aldehydes with dimeredone is as follows (Scheme 4): (1) the reaction of a molecule of enolized dimeredone with aromatic aldehyde activated by the catalyst, which yields intermediate (I); (2) intermediate (I) undergoes dehydration to give the intermediate (II); (3) nucleophilic addition of second molecule

of dimeredone on activated intermediate (II), in the Michael addition fashion, affords uncyclized adduct 2,2'-aryl-methylene bis(3-hydroxy-2-cyclohexene-1-one) (III), which produces 1,8-dioxo-octahydroxanthenes after intramolecular cyclodehydration [10, 11]. As it can be seen from Table 2, aromatic aldehydes bearing the electron withdrawing groups (entries 1,2) react with dimeredone faster than those containing electron releasing groups (entries 10–12). According to the above-mentioned mechanism, this could be due to the greater tendency of the intermediate II to react with dimeredone in the presence of the electron withdrawing groups substituted on arylaldehydes.

To evaluate the level of reusability and recycling of the catalyst, a series of catalytic cycles were run. In each cycle, the catalyst was separated by an external magnet, washed with ethanol, and reused. As shown in Figure 11, the catalyst can be reusable with negligible loss in its activity. The activity loss is probably due to loss of the active sites of catalyst by water or reaction products during separation and washing cycles.

To find out whether the reaction takes place in the solid matrix of Co–Sn–Cu oxides/graphene nanocomposites or whether any other species (simply released in the reaction medium) are responsible in the synthesis of 1,8-dioxo-octahydroxanthenes, Co–Sn–Cu oxides/graphene nanocomposite (0.1 g) was added to a solution of aldehyde (1 mmol) and dimeredone (2 mmol) in EtOH/H<sub>2</sub>O (1:1) and the mixture was stirred at room temperature for 4 h. Then, the catalyst was removed by an external magnet, and the filtrate showed no catalytic activity for the preparation of 1,8-dioxo-octahydroxanthenes. These observations indicate that Co–Sn–Cu oxides/graphene nanocomposites are stable under the reaction conditions; there is no danger of leaching during reactions.

**TABLE 2** Comparison of the efficiencies of a number of different reported catalysts with that of nanocomposite 3 in the reaction of benzaldehyde with dimedone

No.	Reaction conditions	Time (min)	Yield (%) <sup>a</sup>
1	NHSO <sub>4</sub> -SiO <sub>2</sub> , CH <sub>3</sub> CN, reflux	210	95 [9]
2	SmCl <sub>3</sub> , solvent-free, 120°C	540	98 [10]
3	[Et <sub>3</sub> NH][HSO <sub>4</sub> ], solvent-free, 100°C	20	94 [11]
4	Fe <sub>3</sub> O <sub>4</sub> nanoparticles, solvent-free, 100°C	30	89 [12]
5	Mg-Al hydrotalcite, H <sub>2</sub> O, reflux	180	85 [13]
6	Sulfated zirconia, EtOH, 70°C	480	95 [14]
7	Trichloromelamine, solvent-free, 110°C	30	82 [15]
8	Cu(II)-Fur-APTES/GO <sup>b</sup> , EtOH/H <sub>2</sub> O, 50°C	30	95 [16]
9	Cerri ammonium nitrate, 2-propanol, US <sup>c</sup> , 50°C	35	98 [17]
10	Ionic liquid [H-NMP] <sup>+</sup> [HSO <sub>4</sub> ] <sup>-d</sup> , US <sup>c</sup> , H <sub>2</sub> O, room temperature	50	86 [18]
11	Cellulose/Al <sub>2</sub> O <sub>3</sub> -[MeIm]Cl-XAlCl <sub>3</sub> <sup>e</sup> , EtOH, room temperature	25	91 [19]
12	Carbon nanotube-BuSO <sub>3</sub> H, EtOH, room temperature	30	95 [20]
13	Co-Sn-Cu oxides/graphene nanocomposite 3, EtOH/H <sub>2</sub> O, room temperature	20	96

<sup>a</sup>Isolated yield.

<sup>b</sup>Furfural-imine-functionalized graphene oxide-copper oxide.

<sup>c</sup>Ultrasound irradiation.

<sup>d</sup>2-Pyrididonium hydrogen sulfate.

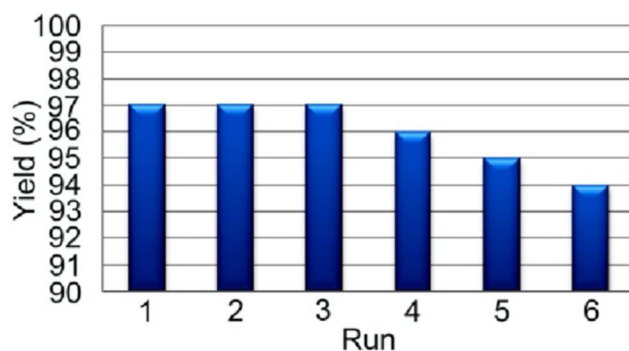
<sup>e</sup>Cellulose aluminum oxide composite supported imidazolium chloroaluminate ionic liquid.

Finally, the catalytic performance of nanocomposite 3 was compared with other catalysts employed for the synthesis of 1,8-dioxo-octahydroxanthenes (Table 2). In addition to having the general advantages attributed to heterogeneous catalysts, nanocomposite 3 has shown superiority over the other catalysts in terms of reaction temperature and time.

### 3.3 | Anti-cancer study

#### 3.3.1 | Effect of nanocomposites on MCF-7 cell proliferation

Some parameters such as shape, size, dimensions, surface structure, density, chemical composition, and solubility play important role for defining the toxicity of nanocompounds [70, 71]. The effective anticancer agents are the compounds that have the most toxicity against cancerous cells whereas the lowest toxicity to normal cells. In this study, to determine the effect of nanocomposites on viability of MCF-7 cells, cells were incubated for 24 and 48 h in the absence or presence of prepared nanocomposites at different concentrations (0–500 µg/mL). The optical density obtained from the absorption at 570 nm was converted to a percentage. Figure 12 shows the reduction of cell viability as concentration increased (dose-dependent). A significant reduction of MCF-7 cell viability was also observed with a time-dependent manner at a specific concentration. Data showed that nanocomposite 1 is more powerful cytotoxic effect than others both in 24 and 48 h. IC<sub>50</sub> (inhibition concentration)

**FIGURE 11** Reusability of nanocomposite 3 (0.1 g) for the reaction of 4-bromobenzaldehyde with two equivalents of dimedone in EtOH/H<sub>2</sub>O (1:1) at room temperature after 20 min

values were measured by probit analysis and were  $61.82 \pm 3.21$ ,  $205.73 \pm 4.25$ , and  $344.03 \pm 6.32$  µg/mL in 24 h, and also  $43.28 \pm 4.28$ ,  $78.83 \pm 5.01$ , and  $135.58 \pm 9.84$  µg/mL in 48 h for nanocomposites 1–3, respectively. Also, IC<sub>50</sub> value for normal cell line was investigated. The human dermal fibroblasts (HDF) line was chosen, and values of IC<sub>50</sub> were measured as  $423.40 \pm 11.53$  and  $444.17 \pm 13.34$  µg/mL for nanocomposites 2 and 3, respectively, in 24 h. In the case of nanocomposite 1, IC<sub>50</sub> value was not observed after this time. IC<sub>50</sub> value was investigated as  $359.2 \pm 13.5$ ,  $92.06 \pm 1.75$ , and  $189.51 \pm 13.59$  µg/mL for nanocomposites 1–3, respectively, in 48 h. The results were shown that nanocomposite 1 has less toxicity against normal cell (as shown in Figure 13). In addition, anti-cancer property of

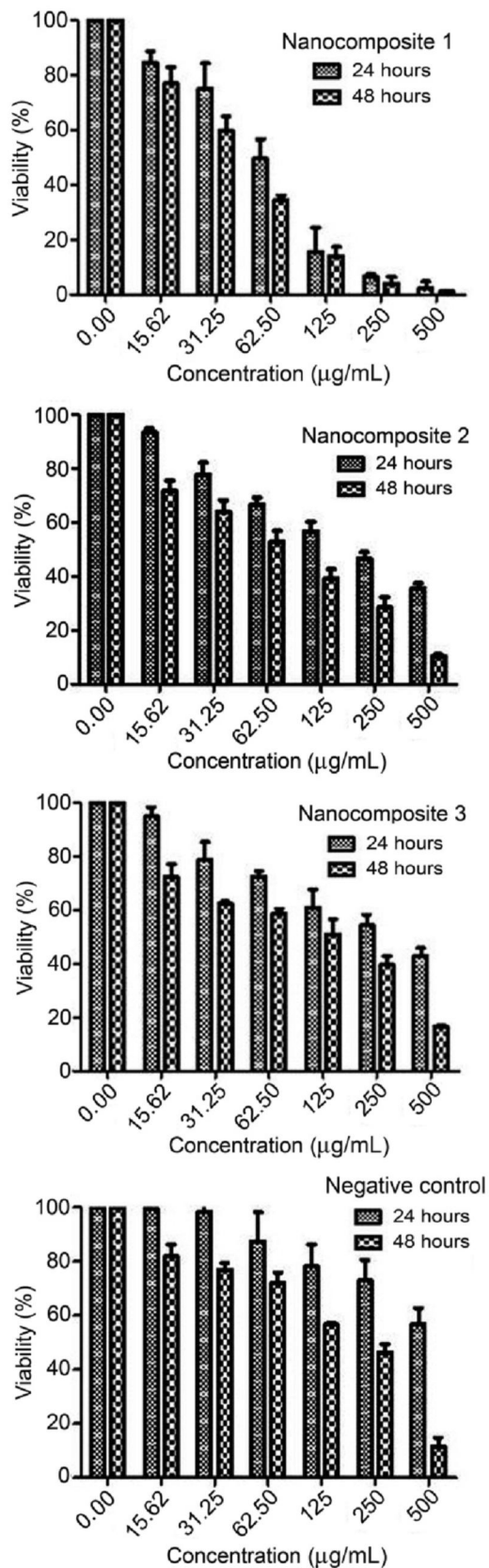


**FIGURE 12** Cytotoxic effect of the nanocomposites and CuO nanoparticle as negative control on MCF-7 cell line by the MTT assay. The data are representative of three independent experiments (mean ± SD)

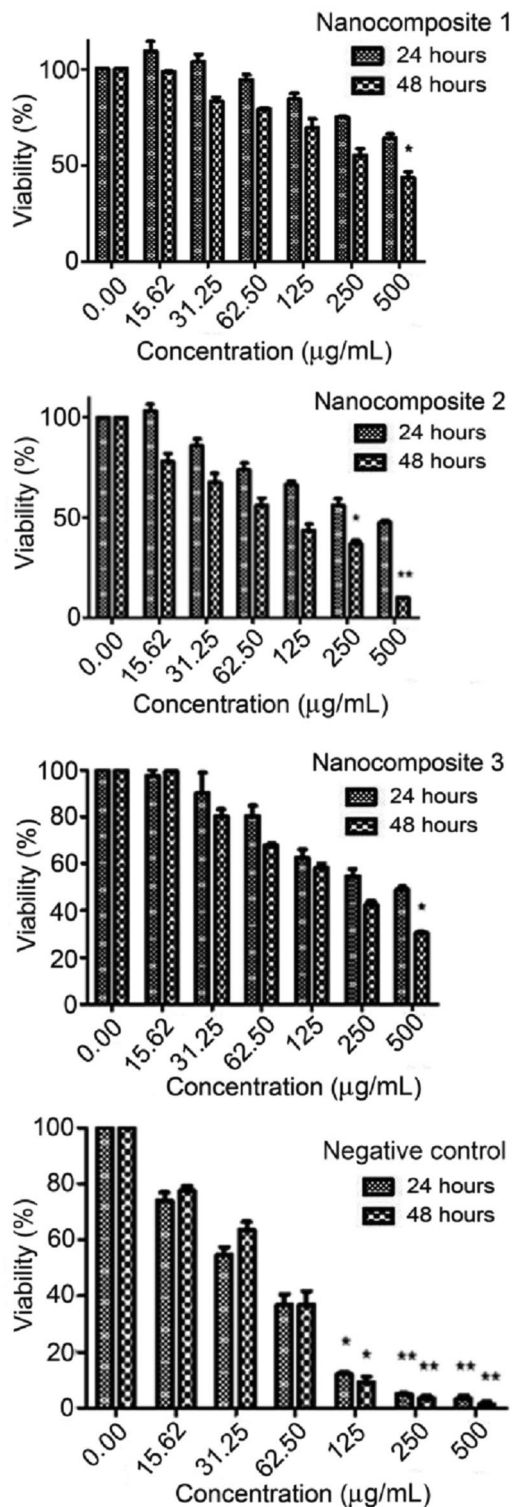


**FIGURE 13** Cytotoxic effect of the nanocomposites and CuO nanoparticle as negative control on HDF cell line by the MTT assay. The data are representative of three independent experiments (mean ± SD)

CuO nanoparticle as negative control [57] was studied against MCF-7 cell line. IC50 value was  $206.36 \pm 10.21$  in 48 h, whereas it was not observed in 24 h. Thus, the presence of Co and Sn in chemical structure (appropriate amount) of these nanocomposites is an effective parameter.

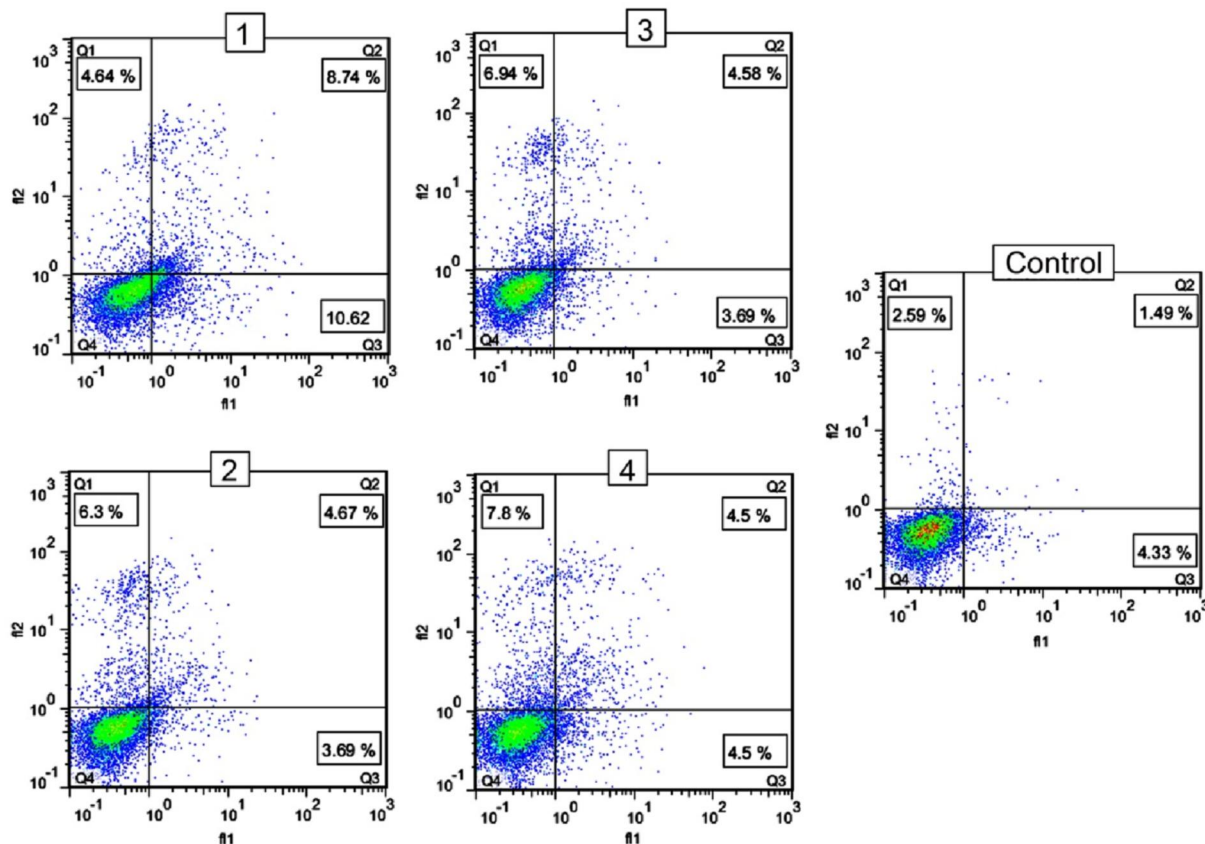


FIGURE 14 Apoptosis induction of the nanocomposites (assigned 1, 2, and 3) and CuO nanoparticle as negative control (assigned 4)

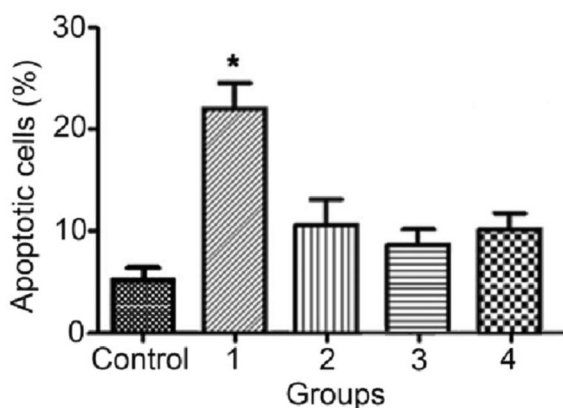


FIGURE 15 Effect of the nanocomposites (assigned 1, 2, and 3) and CuO nanoparticle as negative control (assigned 4) on apoptosis after 48 h. The percentage of cells in early and late apoptosis was considered as apoptosis

### 3.3.2 | Effect of the nanocomposites on MCF-7 cell apoptosis

To assess whether nanocomposites could induce apoptosis in MCF-7 cells, apoptosis induction was determined by an Annexin-V-FITC/PI apoptosis detection kit. MCF-7 cells were incubated for 48 h at IC<sub>50</sub> value. Cells that were positive just for Annexin-V and those that were positive

both for Annexin-V and PI were considered as early and late apoptotic cells, respectively. As shown in Figure 14, nanocomposites could induce apoptosis in treated cell and nanocomposite 1 was more powerful in inducing apoptosis, compared with other nanocomposites and CuO nanoparticle.

Finally, cells were exposed to IC<sub>50</sub> value of nanocomposites for 48 h. Dot plots show the results of a representative apoptosis assay. The number of cells in apoptosis indicated as percentage relative to the total cell number. Treated cells with nanocomposites at IC<sub>50</sub> value showed a significant increase in the amount of apoptotic cells compared with the control group just in nanocomposite 1 (\*P<0.05) (Figure 15).

So far, many investigations were done based on metallic nanoparticles (metal oxides, metallic nanocomposites, magnetic nanoparticles, graphene-based nanoparticles etc.) to find out effective anticancer drugs that play an important role in the apoptosis [72–77]. The presence of anionic phospholipids in cancer cells causes negative zeta potential that absorb into positively charged nanoparticles by strong electrostatic interaction [78, 79]. The nanoparticles cause the inflammation, damage of DNA or cell membrane, and eventually cell death occurs [80]. In this work, we prepared Co–Sn–Cu oxides/graphene nanocomposites, for the first time, via solid-state microwave method as a new, simple, and

fast strategy and their anti-cancer effects in MCF-7 cells were investigated via apoptosis induction. The results showed that nanocomposite 1 was more potent than copper nanoparticles (CuNP, IC<sub>50</sub> = 85 µg/mL) [81], silver nanoparticles (IC<sub>50</sub> = 90 µg/mL) [82], Fe<sub>3</sub>O<sub>4</sub>/Ag nanocomposite (IC<sub>50</sub> = 135 µg/mL) [83], and copper sulfide quantum dots (CuSQDs) loaded nano-GO (IC<sub>50</sub> = 100 µg/mL) [84]. The superiority of our introduced nanocomposites may be due to different factors such as type and ratio of elements that resided in nanocomposite, type of precursor, as well as synthetic method. We anticipate that the solid-state microwave method, used for the preparation of the present nanocomposites 1–3, would be the newly developed route for the synthesis of different anticancer drugs based on nanostructured materials. In addition, as mentioned in the Introduction section, graphene and its derivatives have supreme physicochemical and pharmaceutical properties, which make them good candidate for research in cancer therapy, recently [85, 86]. The biodegradation of graphene nanomaterials by microbes and enzymes has also been documented [87, 88]. Therefore, considering the presence of the Co–Sn–Cu oxides on graphene surface in the presented Co–Sn–Cu oxides/graphene nanocomposites and obtaining very good results in the context of anticancer activity at this stage, we predict that these nanocomposites are potential and promising materials for the preparation of anticancer drugs after taking part in clinical trials.


## 4 | CONCLUSIONS

In this work, we proposed solid-state microwave irradiation as a simple, efficient, safe, fast, and environmental friendly method for the synthesis of pure Co–Sn–Cu oxides/graphene nanocomposites. This method did not require fuel, solvent, surfactant, any expensive materials, and any complex instruments. The nanocomposites were used as green catalysts for preparing 1,8-dioxo-octahydroxanthenes at room temperature. The catalysts can be easily separated from reaction media using an external magnet and are reusable. Simple work-up procedure, easy handling of the catalyst, high yields, and short reaction times are the other obvious advantages of the present method. Following these results, the researchers further investigated anti-cancer activity of the nanocomposites. The results of our study showed that nanocomposites can silence cell proliferation with a time- and dose-dependent manner. Also, the results demonstrated that nanocomposites can induce apoptosis in breast cancer cell line which is an advantageous effect of anti-cancer therapy. The results indicated that nanocomposite 1 was a more powerful apoptosis inducer than other nanocomposites in MCF-7 cells. On the basis of the results, following 48 h incubation, it derived almost 30% of cells to apoptosis at IC<sub>50</sub> value concentrations. Pleasingly, photocatalyst properties of the synthesized nanocomposites are under investigation and will be reported in due course.

## ACKNOWLEDGMENTS

The authors gratefully acknowledge Shahrekord University, Islamic Azad University Shahrekord, Shahrekord University of Medical Sciences, and Research Institute of Petroleum Industry. We thank Mr. Amin Soltani from Shahrekord University of Medical Sciences for his help on the cell viability and apoptosis assays.

## ORCID

*Kaveh Parvanak Boroujeni*  <https://orcid.org/0000-0002-5995-5528>

## REFERENCES

- Julkapli, N.M., Bagheri, S.: Graphene supported heterogeneous catalysts. *Int. J. Hydrogen. Energy.* 40(2), 948–979 (2015)
- Qiao, K., et al.: Effects of graphene on the structure, properties, electro-response behaviours of GO/PAA composite hydrogels and influence of electro-mechanical coupling on BMSC differentiation. *Mater. Sci. Eng. C.* 93, 853–863 (2018)
- Molina-García, M.A., Rees, N.V.: Dual-doped graphene/perovskite bifunctional catalysts and the oxygen reduction reaction. *Electrochem. Commun.* 84, 65–70 (2017)
- Xu, C., et al.: Promotional synergistic effect of Sn doping into a novel bimetallic Sn-W oxides/graphene catalyst for selective oxidation of alcohols using aqueous H<sub>2</sub>O<sub>2</sub> without additives. *Appl. Catal. A.* 558, 26–33 (2018)
- Saada, R., et al.: Greener synthesis of dimethyl carbonate using a novel tin-zirconia/graphene nanocomposite catalyst. *Appl. Catal. B.* 226, 451–462 (2018)
- Librowski, T., et al.: New xanthone derivatives as potent anti-inflammatory agents. *Medicina. (Kaunas).* 41(1), 54–58 (2005)
- Chatterjee, S., et al.: Xanthene derived potent nonpeptidic inhibitors of recombinant human calpain I. *Bioorg. Med. Chem. Lett.* 6(13), 1619–1622 (1996)
- Mulakayala, N., et al.: A greener synthesis of 1,8-dioxo-octahydroxanthene derivatives under ultrasound. *Tetrahedron. Lett.* 53(51), 6923–6926 (2012)
- Das, B., et al.: An efficient synthesis of 1,8-dioxo-octahydroxanthenes using heterogeneous catalysts. *Catal. Commun.* 8(3), 535–538 (2007)
- Ilangovan, A., et al.: A highly efficient green synthesis of 1, 8-dioxo-octahydroxanthenes. *Chem. Cent. J.* 5, 81–86 (2011)
- Zhou, Z., Deng, X.: [Et<sub>3</sub>NH][HSO<sub>4</sub>] catalyzed efficient and green synthesis of 1,8-dioxo-octahydroxanthenes. *J. Mol. Catal. A: Chem.* 367, 99–102 (2013)
- Ghasemzadeh, AM., Safaei-ghomi, J., Zahedi, S.: Fe<sub>3</sub>O<sub>4</sub> nanoparticles: a highly efficient and easily reusable catalyst for the one-pot synthesis of xanthene derivatives under solvent-free conditions. *J. Serb. Chem. Soc.* 78, 769–779 (2013)
- Gupta, R., Ladage, S., Ravishankar, L.: One-pot synthesis of 1,8-dioxo-octahydroxanthenes catalyzed by Mg-Al hydrotalcites. *Chem. J.* 1, 1–4 (2015)
- Kahandal, S.S.: An efficient route to 1,8-dioxo-octahydroxanthenes and-decahydroacridines using a sulfated zirconia catalyst. *Catal. Commun.* 97, 138–145 (2017)
- Maleki, B., et al.: Facile synthesis and investigation of 1,8-dioxo-octahydroxanthene derivatives as corrosion inhibitors for mild steel in hydrochloric acid solution. *New J. Chem.* 40(2), 1278–1286 (2016)
- Mogha, S.N.K., et al.: Fur-imine-functionalized graphene oxide-immobilized copper oxide nanoparticle catalyst for the synthesis of xanthene derivatives. *ACS Omega.* 3, 16377–16385 (2018)
- Mulakayala, N., et al.: Catalysis by molecular iodine: a rapid synthesis of 1,8-dioxo-octahydroxanthenes and their evaluation as potential anti-cancer agents. *Bioorg. Med. Chem. Lett.* 22(6), 2186–2191 (2012)

18. Naeimi, H., Sadat Nazifi, Z.J.: A facile one-pot ultrasound assisted synthesis of 1,8-dioxo-octahydroxanthene derivatives catalyzed by Brønsted acidic ionic liquid (BAIL) under green conditions. *J. Ind. Eng. Chem.* 20(3), 1043–1049 (2014)
19. Parvanak Boroujeni, K., Tahani, P.: The cellulose aluminum oxide composite-supported imidazolium chloroaluminate ionic liquid as a novel and stable heterogeneous catalyst. *Inorg. Nono-Met. Chem.* 47(8), 1150–1156 (2017)
20. Parvanak Boroujeni, K., Heidari, Z., Khalifeh, R.: Carbon nanotube-supported butyl 1-sulfonic acid groups as a novel and environmentally compatible catalyst for the synthesis of 1,8-dioxo-octahydroxanthenes. *Acta. Chim. Slov.* 63(3), 602–608 (2016)
21. Lehn, J.M.: *Comprehensive Supramolecular Chemistry*, 1st edn.. Pergamon Press, Oxford (1995)
22. Barragín, E., et al.: The role of cobalt, copper, nickel, and zinc in the DNA replication inhibitory activity of p-aminophenyl triphenylporphyrin. *Appl. Organometal. Chem.* 18, 311–317 (2004)
23. Byrne, C., et al.: Metals and breast cancer. *J. Mammary Gland Biol. Neoplasia.* 18, 63–73 (2013)
24. Sigel, H.: Metal ions in biological systems. In: Petering, D.H. (ed.) *Carcinostatic Copper Complexes*, Marcel Dekker, New York, pp. 197–229. (1980)
25. Jevtović, V., et al.: Anticancer activity of new copper (II) complexes incorporating a pyridoxal-semicarbazone ligand. *Contemp Mater.* 133–137 (2010). 1–2
26. Cagnoli, M., et al.: Synthesis and biological activity of gold and tin compounds in ovarian cancer cells. *Anticancer Drugs.* 9(7), 603–610 (1998)
27. Pellerito, C., et al.: Synthesis, structural investigations on organotin(IV) chlorin-e6 complexes, their effect on sea urchin embryonic development and induced apoptosis. *J. Inorg. Biochem.* 99(6), 1294–1305 (2005)
28. Li, D.D., Tian, J.L., Gu, W., et al.: DNA binding, oxidative DNA cleavage, cytotoxicity, and apoptosis-inducing activity of copper(II) complexes with 1,4-tpbd (N,N,N',N'-tetrakis(2-ylidylmethyl)benzene-1,4-diamine) ligand. *J. Inorg. Biochem.* 105(6), 894–901 (2011)
29. Chauhan, M., Banerjee, K., Arjmand, F.: DNA binding studies of novel copper(II) complexes containing l-tryptophan as chiral auxiliary: in vitro antitumor activity of Cu–Sn<sub>2</sub> complex in human neuroblastoma cells. *Inorg. Chem.* 46(8), 3072–3082 (2007)
30. Zaidi, Y., et al.: A comprehensive biological insight of trinuclear copper(ii)–tin(iv) chemotherapeutic anticancer drug entity: in vitro cytotoxicity and in vivo systemic toxicity studies. *Metallomics.* 6, 1469–1479 (2014)
31. Chang, E.L., Simmers, C., Knight, D.A.: Cobalt complexes as antiviral and antibacterial agents. *Pharmaceuticals.* 3(6), 1711–1728 (2010)
32. Fantechi, E., et al.: A smart platform for hyperthermia application in cancer treatment: cobalt-doped ferrite nanoparticles mineralized in human ferritin cages. *ACS. Nano.* 8(5), 4705–4719 (2014)
33. Habib, A.H., et al.: Evaluation of iron-cobalt/ferrite core-shell nanoparticles for cancer thermotherapy. *J. Appl. Phys.* 103(7), 3 (2008). 07A307
34. Jing, Y., et al.: Experimental and theoretical investigation of cubic FeCo nanoparticles for magnetic hyperthermia. *J. Appl. Phys.* 105, 3 (2009). 07B305
35. Xu, Y., et al.: Cobalt nanoparticles coated with graphitic shells as localized radio frequency absorbers for cancer therapy. *Nanotechnology.* 19, 9 (2008). 435102
36. Nounou, M.I., et al.: Breast cancer: conventional diagnosis and treatment modalities and recent patents and technologies. *Breast Cancer Basic Clin. Res.* 9, 17–34 (2015)
37. Molaakbari, E., et al.: Synthesis and application of conductive polymeric ionic liquid/nanocomposite to construct a nanostructure based electrochemical sensor for determination of risperidone and methylphenidate. *J. Electroanal. Chem.* 801, 198–205 (2017)
38. Behera, S., Sarkar, R.: Effect of different metal powder anti-oxidants on N220 nano carbon containing low carbon MgO-C refractory: an in-depth investigation. *Ceram. Int.* 42(16), 18484–18494 (2016)
39. Tohidian, Z., Sheikhshoae, I.: Sonochemical, spectroscopic study and antibacterial activity of two uranyl Schiff base complexes in nano scale. *Rend. Fis. Acc. Lincei.* 28(2), 405–413 (2017)
40. Vaigankar, D.C., et al.: Tellurite biotransformation and detoxification by *Shewanellabaltica* with simultaneous synthesis of tellurium nanorods exhibiting photo-catalytic and anti-biofilm activity. *Ecotoxicol. Environ. Saf.* 165, 516–526 (2018)
41. Batra, H., Pawar, S., Bahl, D.: Curcumin in combination with anti-cancer drugs: a nanomedicine review. *Pharmacol. Res.* 139, 91–105 (2018)
42. Gurunathan, S., et al.: Green synthesis of graphene and its cytotoxic effects in human breast cancer cells. *Int. J. Nanomed.* 8(1), 1015–1027 (2013)
43. Wu, J., et al.: Graphene oxide used as a carrier for adriamycin can reverse drug resistance in breast cancer cells. *Nanotechnology.* 23(35), 355101 (2012)
44. Hatamie, S., et al.: Curcumin-reduced graphene oxide sheets and their effects on human breast cancer cells. *Mater. Sci. Eng. C.* 55, 482–489 (2015)
45. Choi, Y.J., Gurunathan, S., Kim, J.H.: Graphene oxide–silver nanocomposite enhances cytotoxic and apoptotic potential of salinomycin in human ovarian cancer stem cells (OvCSCs): a novel approach for cancer therapy. *Int. J. Mol. Sci.* 19(3), 710–732 (2018)
46. Peng, W., et al.: Enhanced anticancer effect of fabricated gallic acid/CdS on the rGO nanosheets on human glomerular mesangial (IP15) and epithelial proximal (HK2) kidney cell lines-cytotoxicity investigations. *J. Photochem. Photobiol. B.* 178, 243–248 (2018)
47. Zhang, Y., et al.: Synthesis and characterization of Tamoxifen citrate modified reduced graphene oxide nano sheets for breast cancer therapy. *J. Photochem. Photobiol. B.* 180, 68–71 (2017)
48. Liu, P., et al.: Platinated graphene oxide: a nanoplatfor for efficient gene-chemo combination cancer therapy. *Eur. J. Pharm. Sci.* 121, 319–329 (2018)
49. Rodrigues, R.O., et al.: Multifunctional graphene-based magnetic nanocarriers for combined hyperthermia and dual stimuli-responsive drug delivery. *Mater. Sci. Eng. C.* 93, 206–217 (2018)
50. Shende, T.P., et al.: Sonochemical synthesis of graphene-Ce-TiO<sub>2</sub> and graphene-Fe-TiO<sub>2</sub> ternary hybrid photocatalyst nanocomposite and its application in degradation of crystal violet dye. *Ultrason. Sonochem.* 41, 582–589 (2018)
51. Zhang, J., et al.: Facile synthesis of Li<sub>4</sub>Ti<sub>5</sub>O<sub>12</sub>/graphene nanocomposites for high performance lithium-ion batteries via a thermal-decomposition reduction in air. *Colloids Surf. A.* 529, 677–685 (2017)
52. Shojaei, M., Nasresfahani, S.h., Sheikhi, M.H.: Hydrothermally synthesized Pd-loaded SnO<sub>2</sub>/partially reduced graphene oxide nanocomposite for effective detection of carbon monoxide at room temperature. *Sens. Actuators B.* 254, 457–467 (2018)
53. Atout, H., et al.: Enhanced photocatalytic degradation of methylene blue: preparation of TiO<sub>2</sub>/reduced graphene oxide nanocomposites by direct sol-gel and hydrothermal methods. *Mater. Res. Bull.* 95, 578–587 (2017)
54. Zhu, Z., et al.: Microwave-assisted hydrothermal synthesis of Ni(OH)<sub>2</sub> architectures and their in situ thermal convention to NiO. *Adv. Powder. Technol.* 22(3), 422–426 (2011)
55. Tohidian, Z., Hashemi, S., Parvanak Boroujeni, K.: Facile microwave-assisted synthesis of NiO nanoparticles and its effect on soybean (Glycine max). *IET Nanobiotechnol.* 13, 101–106 (2019)
56. Ebrahimipour, S.Y., et al.: Synthesis, spectral characterization, structural studies, molecular docking and antimicrobial evaluation of new dioxidouranium(VI) complex incorporating tetradentate N<sub>2</sub>O<sub>2</sub> Schiff base-ligands. *RSC. Adv.* 5, 95104–95117 (2015)
57. Tohidian, Z., et al.: A novel copper (II) complex containing a tetradentate Schiff base: synthesis, spectroscopy, crystal structure, DFT study, biological activity and preparation of its nano-sized metal oxide. *J. Mol. Struct.* 1134, 706–714 (2017)
58. Parvanak Boroujeni, K., Karimi, S., Eskandari, M.M.: Synthesis and application of graphene oxide–supported aluminium chloride as a novel and an environmentally friendly catalyst for the preparation of bis(pyrazolyl)methanes. *Russ. J. Org. Chem.* 55, 694–701 (2019)

59. Chen, C.M., et al.: Chemically derived graphene-metal oxide hybrids as electrodes for electrochemical energy storage: pre-graphenization or post-graphenization? *J. Mater. Chem.* 22(28), 13947–13955 (2012)
60. Klug, H.P., Alexander, L.E.: *X-ray Diffraction Procedures*, 2nd edn. Wiley, New York (1964)
61. Xiong, K., et al.: Flower-like  $\text{CuCo}_2\text{O}_4$ @RGO nanohybrid as an effective counter electrode for dye-sensitized solar cells. *Mater. Lett.* 204, 69–72 (2017)
62. Kumar, S., Nath, M.: New triphenyltin(IV) complexes of flexible tripodal Schiff base ligands: X-ray structural characterization of  $\text{Ph}_3\text{SnCl}$ . (H<sub>3</sub>trensal). *J. Organomet. Chem.* 848, 10–21 (2017)
63. Ding, J., et al.: Low-temperature preparation of magnetically separable  $\text{Fe}_3\text{O}_4$ @CuO-RGO core-shell heterojunctions for high-performance removal of organic dye under visible light. *J. Alloys. Compd.* 688, 649–456 (2016)
64. Aslan, K., Geddes, C.D.: A Review of an ultrafast and sensitive bioassay platform technology: microwave-accelerated metal-enhanced fluorescence. *Plasmonics*. 3(2), 89–101 (2008)
65. Comba, P., et al.: Two different types of folding of isomeric macrocycles induced by metal ion coordination. *J. Chem. Soc. Dalton. Trans.*, 1691–1695 (1997)
66. Lochenie, C., et al.: Water channels and zipper structures in Schiff base-like Cu(II) and Ni(II) mononuclear complexes. *Cryst. Eng. Comm.* 16, 6213–6218 (2014)
67. Gupta, D., et al.: Facile synthesis of  $\text{Cu}_2\text{O}$  and  $\text{CuO}$  nanoparticles and study of their structural, optical and electronic properties. *J. Alloys Compd.* 743, 737–745 (2018)
68. Chen, Y., et al.: Band gap manipulation and physical properties of preferred orientation  $\text{CuO}$  thin films with nano wheatear array. *Ceram. Int.* 44, 1134–1141 (2018)
69. Rayapa Reddy, K.: Green synthesis, morphological and optical studies of  $\text{CuO}$  Nanoparticles. *J. Mol. Struct.* 1150, 553–557 (2017)
70. Wang, E.C., Wang, A.Z.: Nanoparticles and their applications in cell and molecular biology. *Integr. Biol.* 6(1), 9–26 (2014)
71. Rasmussen, J.W., et al.: Zinc oxide nanoparticles for selective destruction of tumor cells and potential for drug delivery applications. *Expert Opin. Drug. Deliv.* 7, 1063–1077 (2010)
72. Goudarzi, M., Salavati-Niasari, M., Amiri, M.: Effective induction of death in breast cancer cells with magnetite  $\text{NiCo}_2\text{O}_4$ / $\text{NiO}$  nanocomposite. *Composites. Part. B.* 166, 457–463 (2019)
73. Toomeh, D., et al.: Minimizing the potential of cancer recurrence and metastasis by the use of graphene oxide nano-flakes released from smart fiducials during image-guided radiation therapy. *Eur. J. Med. Phys.* 55, 8–14 (2018)
74. Firdhouse, M.J., Lalitha, P.: Facile synthesis of anisotropic gold nanoparticles and its synergistic effect on breast cancer cell lines. *IET Nanobiotechnol.* 14(3), 224–229 (2020)
75. Nordin, N., et al.: Characterisation of sol-gel method synthesised  $\text{MgZnFe}_2\text{O}_4$  nanoparticles and its cytotoxic effects on breast cancer cell line, MDA MB-231 in vitro. *IET Nanobiotechnol.* 11(3), 343–348 (2017)
76. Ghassami, E., et al.: HER-2 aptamer-targeted Ecoflex<sup>®</sup> nanoparticles loaded with docetaxel promote breast cancer cells apoptosis and antimetastatic effect. *IET Nanobiotechnol.* 13(4), 426–432 (2019)
77. Izadpanah, M.R., et al.: Functionalization of  $\text{Fe}_3\text{O}_4$  nanoparticles by thiosemicarbazone derivative containing pyrazole fragment enhances the apoptosis of human breast cancer MCF-7 cells. *IET Nanobiotechnol.* (2020). <https://doi.org/10.1049/iet-nbt.2019.0199>
78. Meulenkamp, E.A.: Synthesis and growth of  $\text{ZnO}$  nanoparticles. *J. Phys. Chem. B.* 102, 5566–5572 (1998)
79. Wang, Z.L.: Zinc oxide nanostructures: growth, properties and applications. *J. Phys. Condensed. Matter.* 16(25), R829–R858 (2004)
80. Vivek, R., et al.: Green biosynthesis of silver nanoparticles from *Annona squamosa* leaf extract and its in vitro cytotoxic effect on MCF-7 cells. *Process. Biochem.* 47(12), 2405–2410 (2012)
81. Solairaj, D., Rameshthangam, P., Arunachalam, G.: Anticancer activity of silver and copper embedded chitin nanocomposites against human breast cancer (MCF-7) cells. *Int. J. Biol. Macromol.* 105, 608–619 (2017)
82. Majeed, S., et al.: Green approach for the biosynthesis of silver nanoparticles and its antibacterial and antitumor effect against osteoblast MG-63 and breast MCF-7 cancer cell lines. *Sustainable Chem. Pharm.* 12, 6 (2019). 100138
83. Salehzadeh, A., et al.:  $\text{Fe}_3\text{O}_4$ / $\text{Ag}$  nanocomposite biosynthesised using *Spirulina platensis* extract and its enhanced anticancer efficiency. *IET Nanobiotechnol.* 13(7), 766–770 (2019)
84. Wang, L., Yan, J.: Superficial synthesis of photoactive copper sulfide quantum dots loaded nano-graphene oxide sheets combined with near infrared (NIR) laser for enhanced photothermal therapy on breast cancer in nursing care management. *J. Photochem. Photobiol., B.* 192, 68–73 (2019)
85. Liu, J., et al.: Graphene-based nanomaterials and their potentials in advanced drug delivery and cancer therapy. *J. Controlled. Release.* 286, 64–73 (2018)
86. Yang, K., Feng, L., Liu, Z.: Stimuli responsive drug delivery systems based on nano-graphene for cancer therapy. *Adv. Drug. Deliv. Rev.* 105, 228–241 (2016)
87. Bhattacharya, K., et al.: Biological interactions of carbon-based nanomaterials: from coronation to degradation. *Nanomedicine.* 12(2), 333–351 (2016)
88. Chen, M., Qin, X., Zeng, G.: Biodegradation of carbon nanotubes, graphene, and their derivatives. *Trends Biotechnol.* 35(9), 836–846 (2017)

**How to cite this article:** Parvanak Boroujeni K, Tohidiyan Z, Lorigooini Z, Hamidifar Z, Eskandari MM. Co–Sn–Cu oxides/graphene nanocomposites as green catalysts for preparing 1,8-dioxo-octahydroxanthenes and apoptosis-inducing agents in MCF-7 human breast cancer cells. *IET Nanobiotechnol.* 2021;15:197–211. <https://doi.org/10.1049/nbt.2.12006>